Fall 2017

Tetrameric structure of beta-amylase 2 (BAM2) in Arabidopsis thaliana

Lauren Elizabeth Pope
James Madison University

Tetrameric Structure of Beta-amylase 2 (BAM2) in Arabidopsis thaliana

An Honors College Project Presented to

the Faculty of the Undergraduate

College of Science and Mathematics

James Madison University

by Lauren Elizabeth Pope

December 2017

Accepted by the faculty of the College of Science and Mathematics, James Madison University, in partial fulfillment of the requirements for the Honors College.

FACULTY COMMITTEE:

Project Advisor: Jonathan D. Monroe, Ph.D.,
Professor of Biology, Biology Department

Reader: Timothy Bloss, Ph.D.
Professor of Biology, Biology Department

Reader: Christopher Berndsen, Ph.D.
Assistant Professor, Chemistry Department

HONORS COLLEGE APPROVAL:

Bradley R. Newcomer, Ph.D.,
Dean, Honors College

PUBLIC PRESENTATION

This work is accepted for presentation, in part or in full, at the JMU Honors College Symposium on 12/1/2017.

Table of Contents

List of Figures and Tables

Figures

Tables

Acknowledgements

I would like to thank my advisor, Dr. Jonathan Monroe, for constant support, encouragement, and dedication in every aspect of this capstone project. I would like to acknowledge Dr. Christopher Berndsen for his significant contributions to the advancement of our knowledge of BAM2, for creating the tetramer model of BAM2, and for dedicating time to being a committee member. I thank Dr. Timothy Bloss for his contributions to this project through his involvement on the committee. I would also like to acknowledge Dr. Amanda Storm for her patience and commitment to excellence. This project would have been impossible without the financial and institutional support of the NSF, the American Society of Plant Biologists Summer Undergraduate Research Fellowship, and the JMU Departments of Biology and Chemistry.

Abstract

Plants store starch during the day for use at night. This process of transitory starch degradation is mostly attributable to the β-Amylase (BAM) family, which are starch exohydrolases that cleave the penultimate α-1,4 glycosidic bonds of starch to release maltose. BAM2 was recently characterized as a catalytically active, K^+-requiring tetramer with sigmoidal kinetics and cooperativity. All other catalytically active BAMs display Michaelis-Menten kinetics, no cooperativity, and do not require salt, making BAM2's characteristics intriguing. Due to a lack of a crystal structure, a monomeric homology model of BAM2 was generated using I-TASSER based on a BAM5 from soybean. The monomer model was then used to make a tetramer model based on the homotetrameric crystal structure of sweet potato BAM5 with YASARA. The tetramer model was tested through site directed mutagenesis of conserved residues that were hypothesized to form interfaces between subunits. Two residues, D490 and W456, are perfectly conserved and located in one interface of the tetramer model. Residue F238 is a perfectly conserved residue that would be in another interface of the tetramer model if the model were slightly shifted and more compact. Site directed mutagenesis was used to swap these residues with a different amino acid, and the mutant proteins were purified for use in enzyme activity assays and size analysis by Size Exclusion Chromatography-Multi Angle Light Scattering. BAM2 D490R and BAM2 W456A disrupted tetramerization and catalytic activity. The F238A mutant is dimeric and maintains catalytic activity resembling BAM2 WT, but with a higher K_m. The results of these mutagenesis experiments revealed that activity of BAM2, unlike other active BAMs, is dependent on its quaternary structure and that the starch-binding groove must be held together with residues in interface A for BAM2 to be active.

Introduction

As primary producers, plants reduce carbon through photosynthesis using light energy. However, plants must store a portion of the reduced carbon from the light period for use during the dark period when photosynthesis is not possible (Zeeman et al. 2010). Referred to as transitory leaf starch, this reserve of carbon is synthesized by a suite of enzymes during the day, allowing for a net accumulation of starch in plastids (Baslam et al. 2017; Zeeman et al. 2010). Plants then break down this starch at night into sugars, which are exported for use throughout the plant (Baslam et al. 2017; Zeeman et al. 2010).

Starch has two main components: amylose and amylopectin. Amylose consists of long straight chains of glucose held together by α,1-4 glycosidic bonds. Amylopectin is mostly chains of α,1-4 linked glucose units, but it is more branched due to the presence of α,1-6 glycosidic bonds (Zeeman et al. 2010). Amylose and amylopectin form helices, which contribute to the packing of crystalline and amorphous layers of the starch granule (Zeeman et al. 2010). The dense packing of these layers leads to a large, insoluble granular structure, preventing starch from impacting the osmotic potential of the plastid (Zeeman et al. 2010).

Amylose and amylopectin chains act as the substrates for many different enzymes during the process of transitory starch degradation. One family of starch-degrading enzymes in particular is the β-amylases (BAMs). BAMs are exohydrolases that cleave the penultimate α,1-4 glycosidic bonds of starch to release maltose (Zeeman et al. 2010). Maltose is the major product of transitory starch degradation (Nittyla et al. 2004). However, before BAMs can act on starch to produce maltose, the surface chains of starch must become solubilized. First, the outer chains of starch are phosphorylated by glucan, water dikinase (GWD) followed by phosphoglucan, water dikinase (PWD) (Edner et al. 2010; Ritte et al. 2002; Hejazi et al. 2008). The phosphorylation of

the outer surface of the starch granule disrupts packing of glucan chains to solubilize the helices (Hejazi et al. 2008). Then, helices must be dephosphorylated by phosphoglucan phosphatase for starch metabolism to proceed (Hejazi et al. 2010). The phosphorylation and subsequent dephosphorylation of the outer chains of starch results in a soluble and accessible surface on which degradation by BAMs can occur (Kötting et al. 2009).

In the model plant *Arabidopsis thaliana*, there are nine BAM genes. There is some redundancy in the functions of many starch active enzymes that makes it difficult to clarify the roles of each BAM during transitory leaf starch degradation (Caspar et al. 1991). While the more well-studied BAMs are known to break down starch in plastids at night, there are paralogs of BAMs with different subcellular localizations and functions (Lao et al. 1999; Kaplan and Guy 2005; Kaplan et al. 2006; Li et al. 2009; Monroe et al. 2014; Fulton et al. 2018). BAM1 acts in plastids of guard cells to aid stomatal opening, and is catalytically active at the beginning of the day (Valerio et al. 2011; Horrer et al. 2016). BAM3 is the most well characterized BAM involved in transitory leaf starch degradation, as it is catalytically active at night in chloroplasts of leaf mesophyll cells (Lao et al. 1999; Kaplan and Guy 2005, Fulton et al. 2008; Monroe et al. 2014). BAM5 has no known function but is localized to the cytosol in phloem tissue and can account for up to 80% of total leaf BAM activity under high light conditions (Lin et al. 1988; Caspar et al, 1989; Wang et al. 1995). BAM6 is hypothesized to act in older plants, and may be localized to plastids due to the presence of a putative N-terminal plastid localization peptide (Monroe et al. 2014). In regards to the catalytically inactive BAMs, BAM7 and BAM8 act as nuclear transcription factors (Reinhold et al. 2011, Soyk et al. 2014). BAM4 and BAM9 are both catalytically inactive pseudoenzymes that are plastid localized (Fulton et al. 2008; Li et al. 2009; Monroe unpublished data). BAM2 is a plastid localized BAM that still has no identifiable

function; however, mutant plants lacking BAM2 have a weak starch accumulation phenotype (Fulton et al. 2008; Monroe et al. 2012; Monroe et al. 2017).

Previous publications claimed that BAM2 had very little catalytic activity, concluding that the enzyme might not be active in vivo (Li et al. 2009; Fulton et al. 2008). However, BAM2 possesses all active site residues that other active BAMs share (Monroe et al. 2017). Other non-catalytic BAMs do not possess these shared residues (Fulton et al. 2008). Therefore, it was hypothesized that BAM2 should be catalytically active (Monroe et al. 2017). Analysis of the BAM gene family provides further evidence that BAM2 might have catalytic activity. Within the BAM family, there are two subfamilies (Monroe et al. 2017). Subfamily I contains *BAM1*, *-3*, and *-9*; whereas Subfamily II contains *BAM2*, *-5*, *-4*, *-6*, *-7*, and *-8* (Monroe et al. 2017). *BAM2* may be the ancestral member of subfamily II, as it is found in the earliest land plants, whereas other members of subfamily II are not. Therefore, *BAM2* probably gave rise to catalytically active *BAM5* (Monroe et al. 2017). It is unlikely that BAM2 is inactive because it gave rise to a catalytically active BAM, and BAM2 possesses all the residues required for catalytic activity. In fact, the Monroe lab recently found recombinant BAM2 to be active in the presence of a physiological concentration of KCl (Monroe et al. 2017). Previous publications claiming that BAM2 was inactive did not include any salt in their assay solutions (Li et al. 2009; Fulton et al. 2008). Assays of BAM2 in buffers containing an array of different anions and cations showed that salts containing potassium were the most effective for enzymatic activity (Monroe et al. 2017). Potassium is the most probable catalytic requirement due to its presence in the chloroplast stroma (Finazzi et al. 2015). However, it is still unclear how salt affects the biochemical structure of BAM2, allowing it to act on starch.

Catalytically active BAMs other than BAM2 have typical Michaelis Menten kinetics and a Hill coefficient of about one, indicating no cooperativity (Monroe et al. 1991, Monroe et al. 2017). Surprisingly, studies of BAM2's activity revealed that the enzyme has sigmoidal kinetics with a Hill coefficient >3, displaying cooperativity (Monroe et al. 2017). Enzymes displaying cooperativity and sigmoidal kinetics commonly have multimeric structures or even an allosteric site (Berg et al., 2002, Cuyvers et al. 2012). Enzymes typically have conserved cores and active sites, while the exterior of the protein is more variable (Caffrey et al., 2004). Therefore, a highly conserved surface would hint at a potential allosteric binding site. There is no crystal structure for BAM2, making it difficult to identify any allosteric binding sites or ligands. Therefore, a homology model of BAM2 was formed using I-TASSER, and was analyzed by conservation scores of residues (Monroe et al. 2017). BAM2 possesses a large, highly conserved surface that is 90° from the active site (Monroe et al. 2017). Two glycine residues located in this conserved surface were mutated to methionine, resulting in a significant reduction in catalytic activity (Monroe et al. 2017). Starch has a large structure, and because BAM2 is plastid localized and acts on starch, starch may bind at this highly conserved surface, changing the conformation of BAM2 so as to promote binding of substrate at the active site, resulting in sigmoidal kinetics (Monroe et al. 2017).

Size Exclusion Chromatography-Multi Angle Light Scattering Analysis (SEC-MALS) calculates the molecular weight of a sample of protein in solution, revealing oligomeric complexes that can't be detected with other protein analyses such as SDS-PAGE. SEC-MALS data showed that BAM2 has an average experimental molecular weight of 214.9 kDa in solution, whereas its calculated molecular weight for one monomer is 57.1 kDa (Monroe et al. 2017). The ratio of calculated molecular weight to expected was 3.8:1, which is consistent with BAM2

forming a tetramer in solution (Monroe et al. 2017). It is not yet clear how the protein forms a tetramer, or how the quaternary structure of BAM2 correlates to its function in vivo.

Prior to the publication of Monroe et al. (2017), BAM1 and BAM3 were considered to be the only catalytically active BAMs in plastids with any physiological significance (Lao et al. 1999; Kaplan and Guy 2005; Fulton et al. 2008, Monroe et al. 2014). However, BAM2 now seems to have an unusual set of defining characteristics, which distinguish it from all other BAM proteins, potentially alluding to a unique function. BAM2 knockout mutants show slight accumulation of starch only in older leaves (Monroe et al. 2014); therefore, the catalytic activity of BAM2 found in vitro might overlap with the function of other starch active enzymes in vivo. However, BAM2 is ancestral and is a catalytically active protein that is highly conserved across land plants, suggesting that it may be an integral component in the complexity of starch degradation.

The aim of this study was to further understand BAM2's role in starch degradation through analysis of its unique catalytic and structural properties. In order to examine the structure of BAM2, I first analyzed a model of the BAM2 tetramer, which showed putative locations for interfaces between subunits of the tetramer. I hypothesized that conserved residues in the homology model that were located near interfaces between subunits of the tetramer would be responsible for stabilizing the quaternary structure. I predicted that creating site directed mutants in these residues would disrupt BAM2 tetramerization, and if they did, this would allow us to determine if tetramerization is necessary for catalytic activity.

Methods

Homology Modeling of BAM2

The BAM2 sequence (GenBank OAP06500.1) was submitted to I-TASSER (https://zhanglab.ccmb.med.umich.edu/I-TASSER/), in order to generate a homology model of the protein. This model consisted of only one monomer of BAM2 based on the monomeric crystal structure of BAM5 from soybean (Adachi et al. 1998). The monomer homology model was then used by Dr. Chris Berndsen to generate a tetramer model based on the BAM5 homotetramer crystal structure from sweet potato (Cheong et al. 1995). After energy minimization in YASARA (Version 17.8.15), the tetramer homology model was saved as a .pdb file for observation of key residues.

Sequence Alignment Analysis

Sequence alignments were formative in finding specific residues that would provide us with information on the tetrameric interfaces of BAM2. Sequences of BAM2 were identified using NCBI's BLAST. This was repeated for BAM5, and FASTA files of all of these sequences were downloaded and entered into Clustal Omega (https://www.ebi.ac.uk/Tools/msa/clustalo/) to be aligned. The Clustal Omega output was then visualized using BOXSHADE (version 3.21) to garner a more visually appealing sequence alignment of BAMs from many flowering plants. Residues of interest were confirmed using the BAM2 tetramer homology model in junction with these alignments.

Site Directed Mutagenesis of BAM2

BAM2 cDNA was previously cloned into the pETDUET vector plasmid, allowing for IPTG-inducible expression of BAM2 (Monroe et al. 2017). This plasmid construct served as a template to begin the process of creating site directed mutants of BAM2. Primers for mutagenesis were obtained from Integrated DNA Technologies (Coralville, Iowa) (Table 1), and consisted of ~20 base pairs upstream and downstream of the codon corresponding to the residue of interest. The primers that were designed are shown in Table 1, with the nucleotides that differ from BAM2 WT capitalized. These primers were designed to make the change from one amino acid to another with the fewest changes in nucleotides as possible.

Polymerase Chain Reaction (PCR) was used to mutagenize the BAM2 cDNA in the pETDUET plasmid. The BAM2 D490R PCR reaction consisted of: 120 ng template DNA, 0.33 mM dNTP's, 1 % dimethyl sulfoxide (DMSO), 8 pmol of each forward and reverse primers, 2 % Herculase II Fusion Polymserase (Agilent, Santa Clara, CA), and 1X Herculase II Fusion Buffer. The BAM2 F238A and BAM2 W456A PCR reactions consisted of 75 ng template DNA, 0.2 mM dNTP's, 1 % DMSO, 8 pmol of each forward and reverse primers, 0.6 U Phusion Hot Start II DNA Polymerase (ThermoScientific, Waltham, MA), and 1X Phusion GC Buffer. Forward and reverse primers for each PCR reactions were heated separately at 95 ^{o}C for 5 min before being added to the PCR mix. PCR reactions (10 μL) were set in a T100 Thermocycler (BioRad, Hercules, CA) with specific protocols containing annealing gradients for optimization of PCR results. The complete protocol for the BAM2 D490R mutant was: 95 ^{o}C for 3 min, then 20 cycles of 95 ^{o}C for 30 sec, an annealing gradient between 64.6 ^{o}C and 74.6 ^{o}C for 1 min, with an extension temperature of 72 ^{o}C for 10 min, and a final extension step of 72 ^{o}C for 10 min. The PCR protocols for BAM2 F238A and BAM2 W456A were: 98 ^{o}C for 30 sec, followed by 20

cycles of 98 °C for 10 sec, an annealing gradient between 72 °C and 60 °C for 20 sec, and an extension period at 72 °C for 4 min, with a final extension step of 72 °C for 10 min.

PCR products were digested with 0.025 U of DpnI so as to degrade any template DNA. Then a 5 uL sample consisting of 1 uL of the digested PCR product in a loading dye were analyzed using gel electrophoresis. The gel reservoir was filled with covered in 8 M Tris base, 5% Acetic Acid, 0.05 mM EDTA pH 8, and was run for ~30 min at 100 V, stained with Ethidium Bromide, and imaged under UV light. The PCR products that were represented by a band at ~7 kb, the calculated size of the pET-DUET plasmid with a BAM2 insert, were transformed into DH5α cells.

Transformation of PCR products into *E. coli*

Competent *E. coli* DH5α cells were prepared according to Inoue et al. (1990), and 50 µL of cells were mixed with 1.5 µL of DpnI digested PCR product. This mix was incubated on ice for 30 min, followed by heat shocking at 42 °C for 90 sec. The tubes were placed on ice for 2 min, then 300 µL of LB broth was added. The tubes were then shaken at 37 °C for one hour, then spread on LB agar plates containing 10 mg/mL carbenicillin and incubated at 37°C.

Table 1. Primers for Site Directed Mutagenesis

F238A

WT cDNA sequence	3'-gactgctcttgaggtttactttgattacatgagaagctttcg -5'
Forward Primer (3'->5')	3'-gactgctcttgaggtttacGCtgattacatgagaagctttcg -5'
Reverse Primer (5'->3')	3'-gaaagcttctcatgtaatcaGCgtaaacctcaagagcagtcc-5'

W456A

WT cDNA sequence	3'-gcaggtgctgaatgctgcttgggatgctagtatacctgttgc -5'
Forward Primer (3'->5')	3'-gcaggtgctgaatgctgctGCggatgctagtatacctgttgc-5'
Reverse Primer (5'->3')	3'-caacaggtatactagcatcCGcagcagcattcagcacctgcc -5'

D490R

WT cDNA sequence	3'-aagcccttaccgatcctgatggtcgccacctttcatgtttc -5'
Forward Primer (3'->5')	3'-aagcccttaccgatcctCGtggtcgccacctttcatgtttc-5'
Reverse Primer (5'->3')	3'-gaaacatgaaaggtggcgaccaCGaggatcggtaaggggctttg-5'

Miniprep for Sequencing

A colony from each of the mutant transformant plates was added to LB broth containing 0.1 mg/mL Carbenicillin and was incubated for 12 hours at 37 °C in a shaking incubator. Then the plasmids were extracted from the culture through a miniprep, in which the cells were centrifuged, and then supernatants were discarded to concentrate the pellet of cells. Cells were resuspended in 50 mM glucose, 25 mM Tris pH 8.0, 10 mM EDTA containing 0.0025 mg RNAse A. The samples were vortexed and then 200 µL of 1% SDS, 0.2 M NaOH was added and mixed in by inversion. The samples stood on ice for 5 min and then 150 µL of 3 M K^+, 5 M acetate was added. The tubes stood on ice for another 5 min, then were centrifuged for 5 min at 3200 x g. To 400 µL of the supernatant, 400 µL of 100% isopropanol was added and tubes stood at room temperature for 2 min. The samples were centrifuged for 5 min at 3200 x g, and supernatants were discarded. Then 200 µL of 100% ethanol was added. Tubes were inverted then centrifuged for 2 min at 3200 x g. Supernatants were discarded, then centrifuged for 10 sec to expel as much ethanol as possible. After allowing all the remaining ethanol to evaporate, the pellet of DNA was suspended in deionized H2O. The concentration of was measured with the nanospectrophotometer, and the DNA was diluted to 100-200 ng/µL. DNA samples were sent to Eurofins Genomics (Louisville, KY) for sequencing. Once the sequences were confirmed to have their respective mutation, the miniprepped DNA from DH5α cells was transformed into BL21+ cells. The BL21+ cells were streaked onto a new plate the day before the transformation. On ice, 250 µL of 50 mM $CaCl_2$ was pipetted into 1.5 mL tubes. A few BL21+ colonies were picked from the plate and suspended in the $CaCl_2$ solution. Colonies were suspended by vortexing, and then miniprepped DNA was added to a final concentration of 40 ng/µL. The tubes were incubated on ice for 15 min, and then were incubated in a 42 °C water bath for 90 s. Then the

tubes were incubated on ice for a 1 min before adding 250 µL of LB broth. This stood at 37°C for 30 min and was plated as described previously.

Nickel Affinity Column Protein Purification

The transformed BL21+ *E. coli* cells were then used to start the process of protein purification. A few transformed colonies were suspended in 3 mL of LB broth containing 0.1 mg/mL carbenicillin, and were grown in a shaking incubator for 12 hours at 37°C. The 3 mL cultures of transformed colonies were then combined with 250 mL of LB broth containing 0.1 mg/mL carbenicillin, and was shaken at 37°C until it reached an OD at 600 nm of 0.4 then IPTG was added to a final concentration of 1mM. The flask was then moved to a 20 °C shaking incubator overnight. The next day, cells were centrifuged into a pellet at 8000 x g for 5 min, then frozen at -20 °C. The pellet was then thawed and suspended in 30 mL of binding buffer (50 mM NaH_2PO_4 pH 8, 0.3 M NaCl, 10 mM imidazole). Cells were lysed while on ice by sonication for 1 min 30 sec, with 5 sec bursts followed by a rest period of 20 sec. The suspension was centrifuged for 15 min at 10,234 x g at 4 °C, then the supernatant was transferred to a new 50 mL tube. Then, 300 µL of an 80% Nickel-nitrilotriacetic acid agarose His-bind resin (QIAGEN, Germantown, MD) slurry was added to the supernatant, and was gently shaken at 4 °C for 1.5 hrs. The tubes were then centrifuged at 1,150 x g for 5 min at 4 °C. The supernatant was discarded and binding buffer was added to bring the bead mixture back up to 10 mL. Then the tubes were centrifuged again for 5 min at 1,150 x g at 4 °C, and the supernatant was again discarded. The beads, with about 5 mL of the supernatant, were added to a 5 mL column (Agilent), and were then washed with 20x the bead volume of wash buffer (50 mM pH 8 NaH_2PO_4, 0.3 M NaCl, 40 mM imidazole).Once the wash buffer had run completely through the

column, 10x the bead volume of elution buffer (50 mM pH 8 NaH_2PO_4, 0.3 M NaCl, 200 mM Imidazole) was added to the column, and the flow through was collected in a beaker on ice.

A dialysis buffer was made containing 20 mM MOPS 7.0, 0.2 M NaCl, and 0.5 mM of TCEP reducing agent (tris (2-carboxyethyl) phosphine). Dialysis tubes were cut and soaked in dialysis buffer for ~10min. Samples were placed in dialysis tubes, submerged in dialysis buffer and gently stirred at 4 °C for 12 hours. The dialysis buffer was replenished with fresh buffer the next morning and was left for another 3 hours.

The dialyzed proteins were then transferred into a 5 mL concentrator column (Amicon) and centrifuged for 3500 x g for 15 min at 4 °C. Then the contents of the column were mixed briefly with a pipette, followed by re-centrifugation for 10 min at 3000 x g and 4 °C. This was repeated at shorter intervals of time until the final volume was about 250 µL. The concentrated protein was transferred to a 1.5 mL tube and centrifuged for 5 min at 3200 x g to pellet out any solids, then aliquoted and stored at -80 °C.

Protein concentrations were determined spectrophotometrically using the BioRad Protein Assay Kit with Bovine Serum Albumin (BSA) as the standard. Purity levels of proteins were assessed using 10% acrylamide SDS PAGE. Either 5 µL of pure protein or of the sample from various stages of the purification process was mixed with SDS sample buffer (0.5M Tris pH6.8, 10% glycerol, 10% SDS, 5% mercaptoethanol, 2.5% bromophenol blue), then boiled for 5 min before being loaded into wells. Gels were run at 100 V of DC current for ~45 min in a buffer of 25 mM Tris base, 192 mM glycine, 0.1 % SDS, then stained with Coomassie Blue G-250 for 12 hours, then de-stained with 45% MeOH, and 10% glacial acetic acid for three hours before imaging in ImageLab (BioRad).

Enzymatic Activity Assays

After each protein was purified, their kinetics were analyzed in assays containing levels of soluble starch (up to 100 mg/mL), as well as 10 mM MES 6.0, and 100 mM KCl. Purified enzyme was suspended in 50 mM MOPS, pH 7.0, 1 mg/mL porcine gelatin, and was vortexed before 50 µL was added to start the assay. Each trial consisted of boiled control assays that instantly denatured the enzyme, as well as two active assays. The assays ran for 20 min before being boiled to terminate the assay. A 25:1 ratio of Copper Reagent A : Copper Reagent B was prepared according to Nelson (1944), and 500 µL was added to each assay. Then, the tubes were boiled for 15 minutes, followed by the addition of 500 µL of arsenomolybdate color reagent (Nelson 1944), in order to visualize reducing ends of sugars. The tubes were vortexed and diluted with 3 mL of H2O before being inverted and subsequently centrifuged for 5 min at 2000 x g and 24 °C. Absorbance values were measured from each assay at 660 nm, which were used to calculate activity rates. The standards were various concentrations of maltose.

The effect of KCl concentration on activity of protein was tested with reactions similar to what was described previously, except with 100 mg/mL of soluble starch and varying levels of KCl (0-100mM).

Size Exclusion Chromatography Multi Angle Light Scattering (SEC MALS)

Multi Angle Light Scattering (MALS) analysis was used to determine the molecular weight of the proteins in solution. Calculated molecular weights and extinction coefficients of each mutant were identified using the ExPASy server's Protein Identification and Analysis Tools (Gasteiger et al., 2005). The 4.6 x 300 mm size exclusion column had a particle size of 5 µm and a pore size of 300 Å. The column was prepared for analysis with a series of sterile, 0.2 µm

filtered buffers. First, 10% methanol was run through the instrument for 12 hours at 0.1 mL/min. Then, diH2O at 0.1 mL/min was run for 12 hours. Finally, 10 mM MOPS 7.0, 250 mM KCl was run at 0.1 mL/min for 12 hours before being accelerated to 0.5 mL/min for three hours. A sample of 0.04 mg of protein in 20µL autoclaved deionized H2O was injected per trial, and each protein was analyzed in triplicate. Absorbance values of samples were measured at 280 nm and 212 nm with an Agilent G1315B Diode Array detector. Light scattering values of samples were measured with a miniDAWN-TREOS (Wyatt 571 Technologies). ASTRA (version 6.1.5.22) was used for analyzing each trial.

Results

Homology Modeling of the BAM2 Tetramer

Recent studies revealed BAM2's tetrameric structure through SEC-MALS analysis (Monroe et al. 2017). Due to a lack of a BAM2 crystal structure, a homology model was generated with I-TASSER, which was used by Dr. Chris Berndsen to construct a tetramer model based on the sweet potato (*Ipomoea batatas)* BAM5 crystal structure (Cheong et al. 1995). This structure was energy minimized in YASARA, revealing a hypothesized structure of the BAM2 tetramer (Figure 1). Each subunit of BAM2 contains an $(\beta/\alpha)_8$ fold (Figure 1). There are also various flexible and disordered regions (Figure 1). In the BAM2 tetramer model, the four subunits of BAM2 are situated in a dimer of dimers conformation, with two distinct interfaces, labelled A and B (Figure 1). Interface A is where two subunits come together to create a deep groove where the putative surface binding site of two subunits face each other. Interface A appears to consist of residues 80-86 and 485-491 from alpha helices and variable regions in the two subunits that form a dimer. Interface B brings together two dimers to form a tetramer. There are many residues that appear in interface B, but in the tetramer model this interface is not that close, making it difficult to define which residues are directly forming Interface B. However, interface B also seems to incorporate residues from alpha helices and a few variable loops.

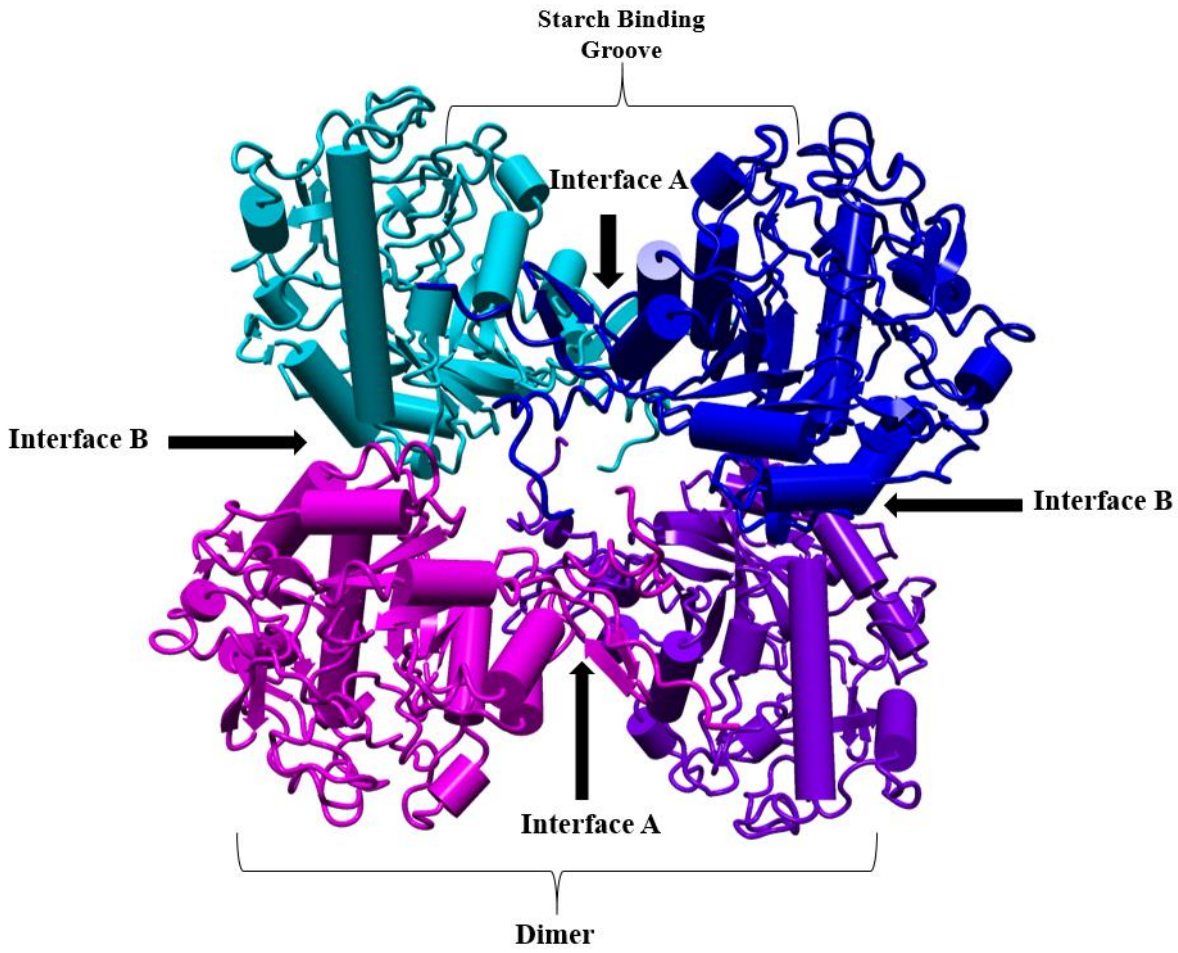

Figure 1. Tetramer Model of BAM2. This BAM2 tetramer model was created with I-TASSER and YASARA based on sweet potato BAM5. Each of the four subunits is a monomer of BAM2, which are individually colored. There are two types of interfaces labeled. Interface A places two starch binding surfaces of adjacent subunits facing each other to form a groove. Interface B places two dimers together in a dimer of dimers conformation.

Sequence Alignments of Residues near Interfaces

In order to determine if any residues in the hypothesized interface regions were conserved, sequence alignments of BAM2 and BAM5 across flowering plants were analyzed (Figure 2). The BAM2 tetramer model shows two distinct interfaces (Figure 1). However, the tetramer model only produced a hypothesized structure. Therefore, the sequence alignments revealed highly conserved regions of the peptide sequence that are most likely to stabilize the tetramer interfaces. Residues hypothesized to be in the interfaces of BAM2 are all generally well conserved (Figure 2). There are also several distinct residues of interest within these sequence alignments due to their conservation trends. Phenylalanine 238 (F238) is perfectly conserved across orthologs in flowering plants, but is variable in the BAM5 ortholog's corresponding position (Figure 2). Tryptophan 456 (W456) is perfectly conserved in BAM2 as well as BAM5 (Figure 2). Aspartic acid 490 (D490) is perfectly and uniquely conserved in BAM2 paralogs, and is a proline in BAM5 (Figure 2).

Targets of Mutagenesis for This Study

To test the validity of the tetramer model, several residues in the putative interfaces that were well conserved were chosen for mutagenesis. For example, residue D490 appears to be a part of interface A (Figure 2), and it is perfectly conserved in BAM2 across land plants (Figure 3). The aromatic residue W456 also appears to have the potential of interacting in interface A (Figure 2), but differs from D490 as it is also perfectly conserved in BAM2 and BAM5 (Figure 3). Residue F238 does not appear to directly make contact between two subunits (Figure 2). However, F238 is perfectly conserved and unique to BAM2 (Figure 3), and is most likely to

interact in BAM2 if the subunits are actually closer in proximity, leading to the hypothesis that it may play a role in the interface B that the tetramer model does not accurately portray. In general, perfectly conserved amino acids that are unique to BAM2 near the apparent interfaces in the BAM2 tetramer model were hypothesized to be integral in tetramerization of the mature BAM2 protein. Because BAM2 is the only known tetrameric BAM, uniquely conserved residues that are near the apparent interfaces in the tetramer model were hypothesized to be important for the formation of BAM2's tetrameric structure.

Purification of Mutant and Wild Type Protein

In an effort to isolate WT recombinant BAM2 protein, as well as individual site directed mutants in the conserved residues of interest, a previously constructed pET-DUET plasmid containing BAM2 cDNA (Monroe et al. 2017) was mutagenized using QuikChange mutagenesis. The resulting plasmid contained an IPTG inducible promoter, the BAM2 cDNA insertion with the appropriate mutation, and a 6-His tag, and a carbenicillin resistance gene, all of which would be utilized for the process of protein purification (Figure 3). A representative analytic gel from the mutagenesis of BAM2 D490R showed a band at ~7kb, the size of the plasmid of interest (Figure 4). The DNA was transformed into E. coli, and the mutations were confirmed by sequencing.

Samples from each step of the process of protein purification were analyzed by an SDS PAGE in order to evaluate the process of protein purification. Figure 5 shows one representative SDS-PAGE gel from the purification of BAM2 D490R. The expected size of the denatured protein was 57kDa. As seen by the prominent band in lane 7 of the expected size, the protein of

the correct size was successfully isolated (Figure 5). All proteins that were purified were at least 90% pure, visualized via SDS PAGE (Figure 6).

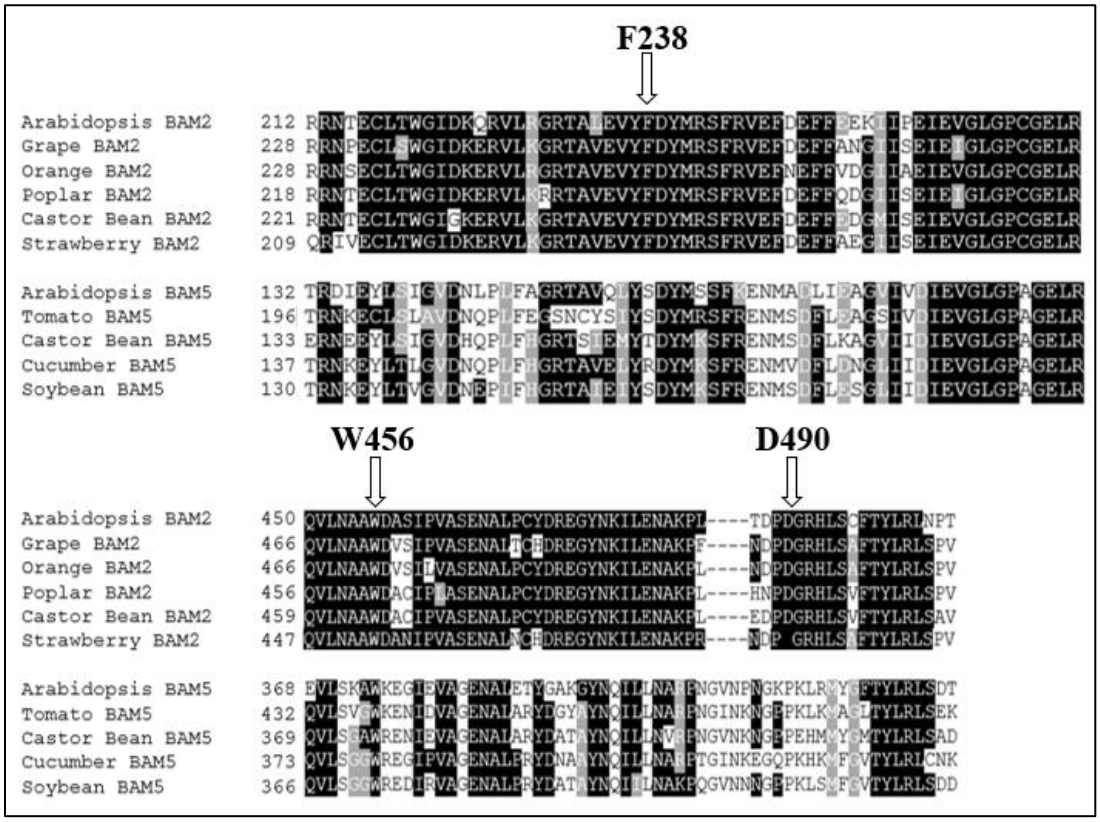

Figure 2. Multiple Sequence Alignment of BAM2 and BAM5 Orthologs from Flowering Plants. Sequence alignments near the residues of interest from the homology model, F238, W456, and D490, show high conservation. On the left are the common names of each genome from which the ortholog's sequence originated. The amino acid number where the sequences begin is to the left of each block of sequence alignment. White text on black background represents >50% conservation among all sequences in the alignment, white on grey background represents similarity, but no specific conservation at a residue, and black text on white background represents a lack of conservation completely.

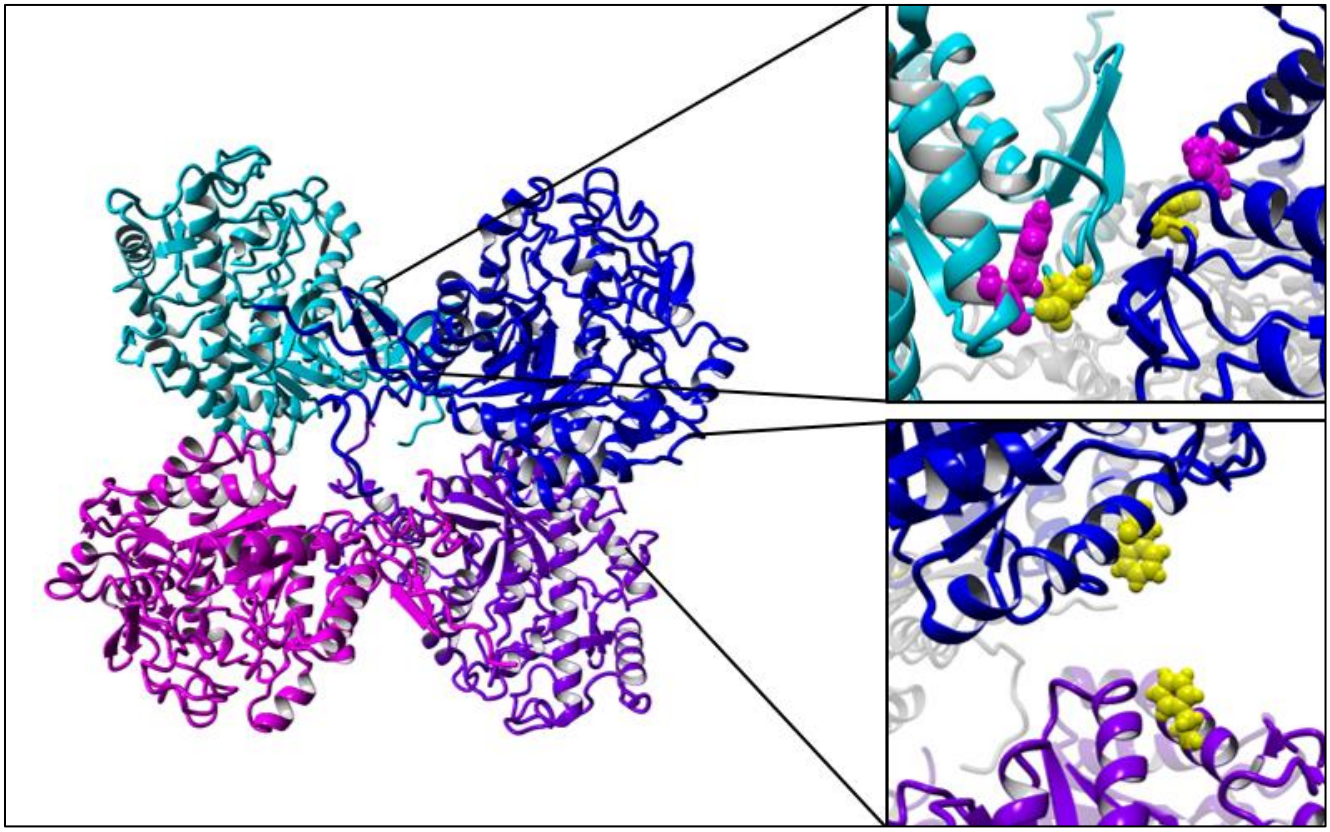

Figure 3. Tetramer Model of BAM2 Highlighting Residues Mutagenized in This Study. On the left is the complete tetramer model, with different subunits of BAM2 represented by different colors. On the upper right are the residues in interface A that may be involved in tetramer formation (D490 in magenta, W456 in yellow) and the bottom right shows F238 (yellow), a residue of interest that may be involved in interface B.

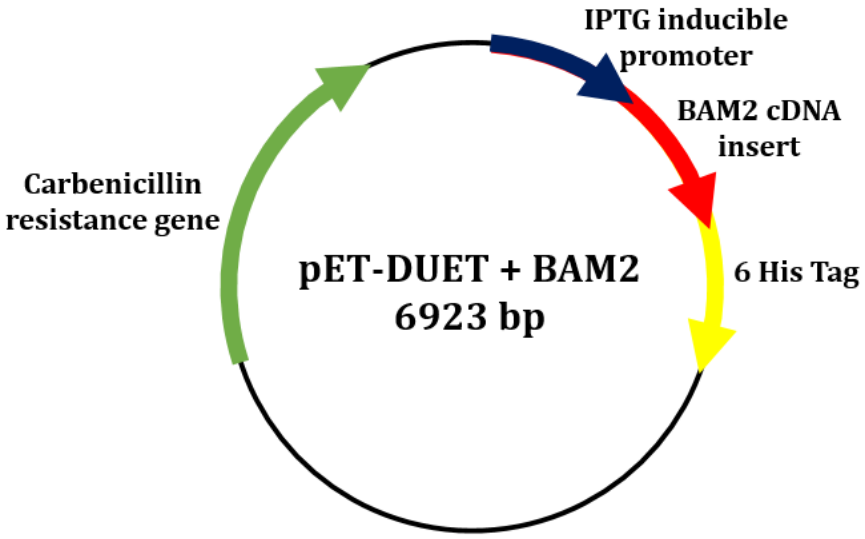

Figure 4. Plasmid map of pET-DUET with BAM2 cDNA insertion. The size of the plasmid is 6923bp, and it contains a carbenicillin resistance gene, an IPTG inducible promoter, the BAM2 cDNA insert, and a 6-His tag, for isolation of transformed *E.coli* as well as purification of protein.

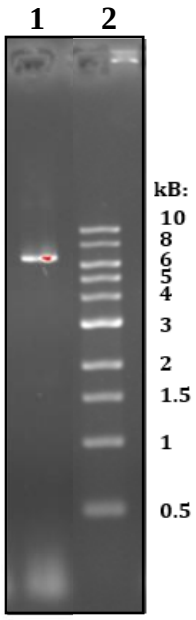

Figure 5. Agarose gel analysis of BAM2 cDNA in pET-DUET with D490R primers. Lane 1 contains the BAM2 D490R PCR products. Lane 2 the 1 kB marker. The expected size of the plasmid construct is 6.9 kB.

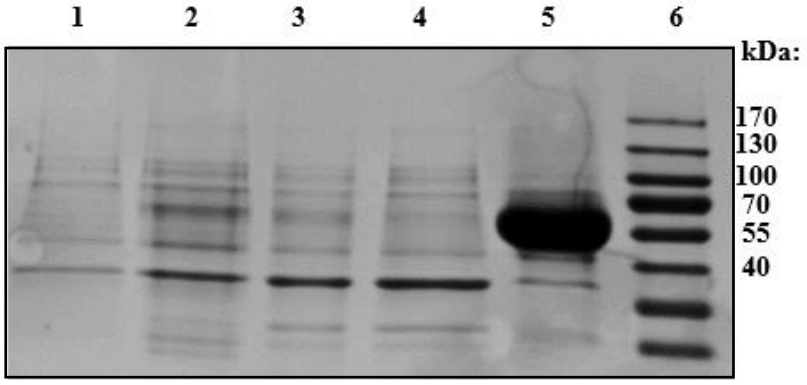

Figure 6. SDS PAGE analysis of the process of protein purification for BAM2 WT.
Expected size of protein is 57 kDa. Lane 1: cell culture before induction with IPTG. Lane 2: cell culture after induction with IPTG. Lane 3: supernatant after sonication and centrifugation. Lane 4: supernatant after bead binding and centrifugation. Lane 5: pure protein. Lane 6: marker.

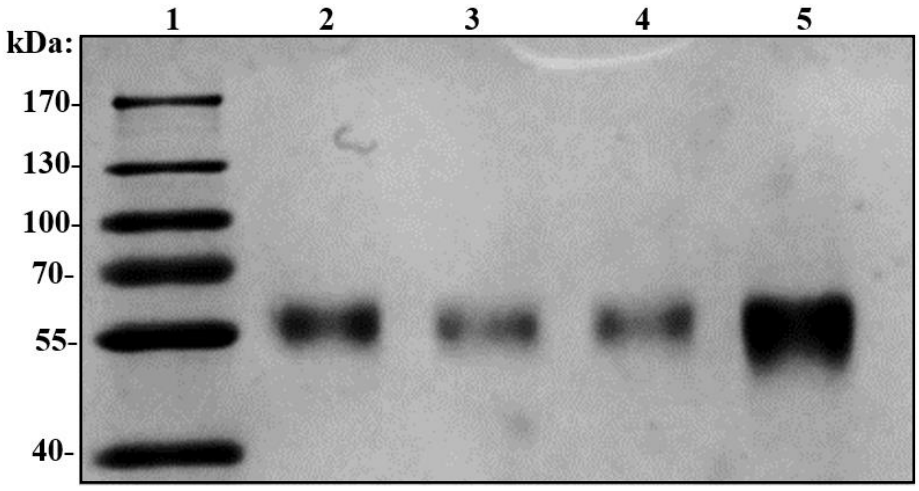

Figure 7. SDS PAGE of Purified BAM2 proteins. Lane 1 has the marker, and each lane following contains 0.5 µg of the pure BAM2 proteins, except for lane 5 which contained 1.0 µg. All lanes showed a band at the expected size of 57kDa, with BAM2 WT in lane 2, BAM2 D490R in lane 3, BAM2 F238A in lane 4, and BAM2 W456A in lane 5.

SEC-MALS Analysis of Mutants

One of the aims of this study was to validate the tetramer model of BAM2 WT through site-directed mutagenesis of residues hypothesized to be located in the interfaces between subunits. It was predicted that these residues may play a role in tetramer formation. It was also predicted that BAM2 could be active if tetramerization was disrupted, as sweet potato BAM5 crystallized as a tetramer, yet is active as a monomer in solution (Cheong et al. 1995). SEC-MALS separated samples of protein by size and calculated molecular weights to show which mutants maintained a tetrameric quaternary structure. SEC-MALS demonstrated that wild type BAM2 is a tetramer with molecular weight averaging around 207.0 kDa. However, the BAM2 W456A and BAM2 F238A mutants were both dimeric with average molecular weights of 135.8 kDa and 143.8kDa, respectively (Figure 8). BAM2 D490R averaged a molecular weight of 59.5 kDa, consistent with it being a monomer (Figure 8).

Catalytic Activity of Mutants

The enzyme activity of each mutant was compared with the wild type using a colorimetric assay (Nelson 1944). The F238A mutant had activity that was similar to WT, but W456A had negligible activity, and D490R had around eight-fold less activity than wild type BAM2 (Figure 9). Because the F238A mutant was the only mutant that had any significant activity, its kinetics were evaluated compared to wild type. Unfortunately, the kinetics data were variable for the BAM2 F238A mutant. These assays must be repeated; however, general trends in the data show that the Km of F238A is higher than wild type (Table 2). We also tested the

BAM2 F238A mutant's requirement of KCl, to reveal that it does still need KCl to be active (Figure 11).

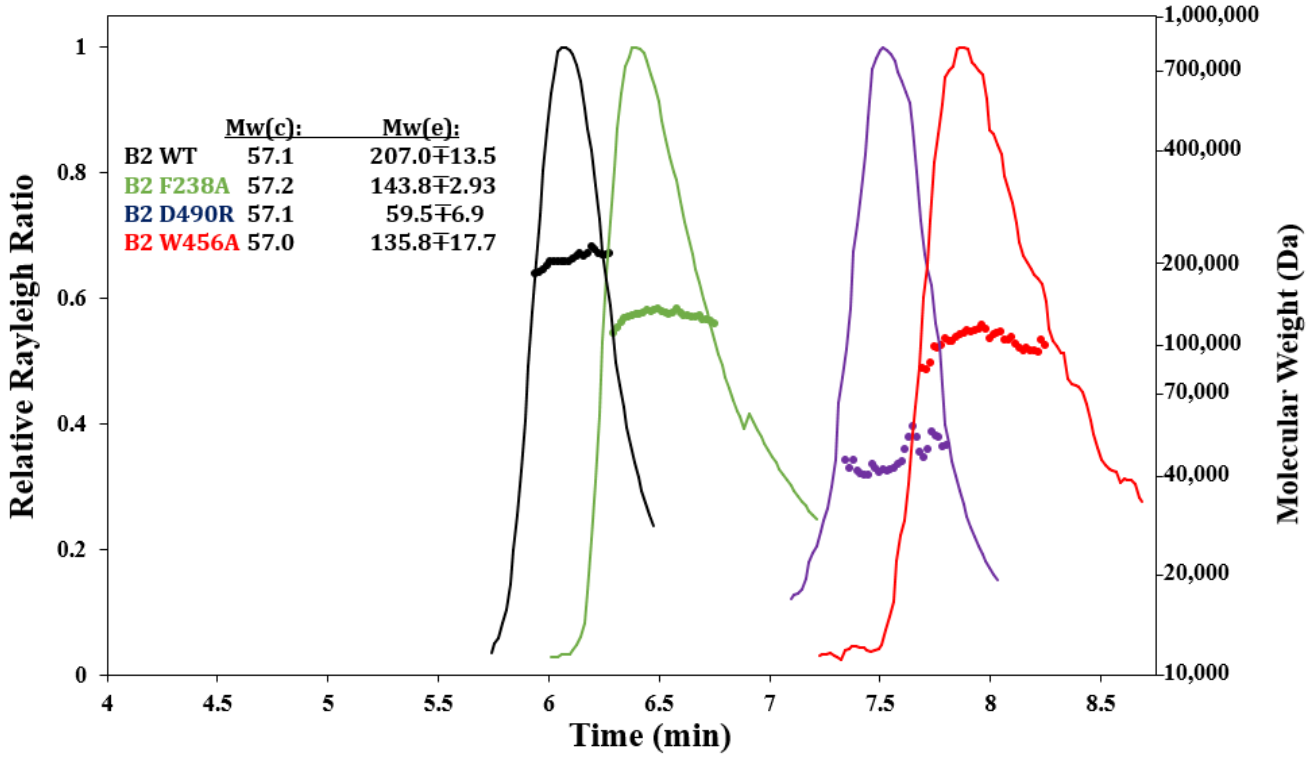

Figure 8. SEC-MALS analysis of BAM2 WT and Mutants. The X-axis shows the time the sample eluted from the column. The primary Y axis shows the relative Rayleigh ratio of light scattering. The secondary Y axis shows the molecular weight of the sample in Daltons. Each peak is colored, WT is black, F238A is green, D490R is blue, and W456A is red. The table to the left of the plot shows calculated molecular weight (Mw(c)) and experimental molecular weight (Mw(e)) in kDa (n=3).

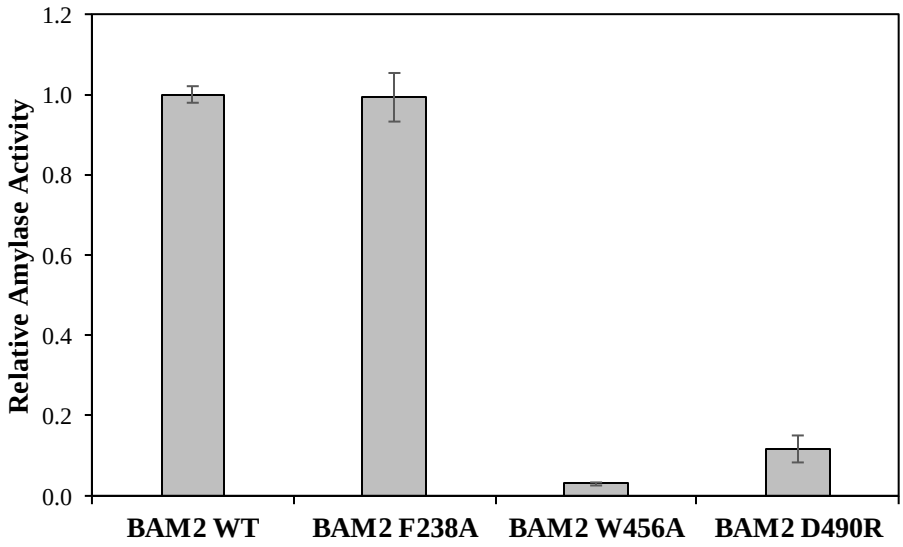

Figure 9. Activity of BAM2 WT, BAM2 F238A, BAM2 D490R, and BAM2 W456A. Activity was calculated for each enzyme in nmol maltose min^{-1} mg^{-1} protein after assays were run for 20 min, and then normalized to BAM2 WT activity. Error bars show one standard deviation above and below the average (n=3).

Table 2. V_{max} and K_m of BAM2 WT and BAM2 F238A

	BAM2 WT (n=3)	**BAM2 F238A (n=2)**
V_{max}	**148.22 ± 8.71**	**283.09 ± 95.16**
K_m	**39.79 ± 0.95**	**113.83 ± 32.82**

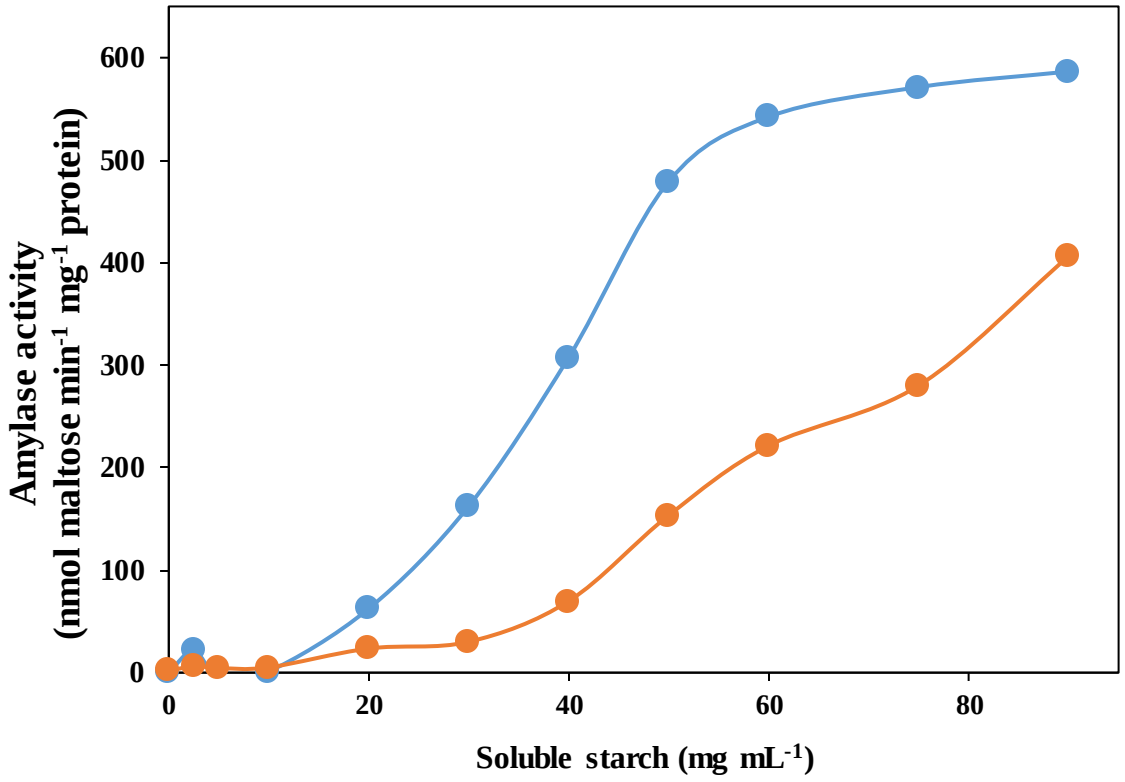

Figure 10. Kinetics of BAM2 WT and F238A. Catalytic activity of BAM2 WT and BAM2 F238A was measured at varying levels of starch using an enzyme activity assay. BAM2 WT is shown in red, while BAM2 F238A is shown in blue.

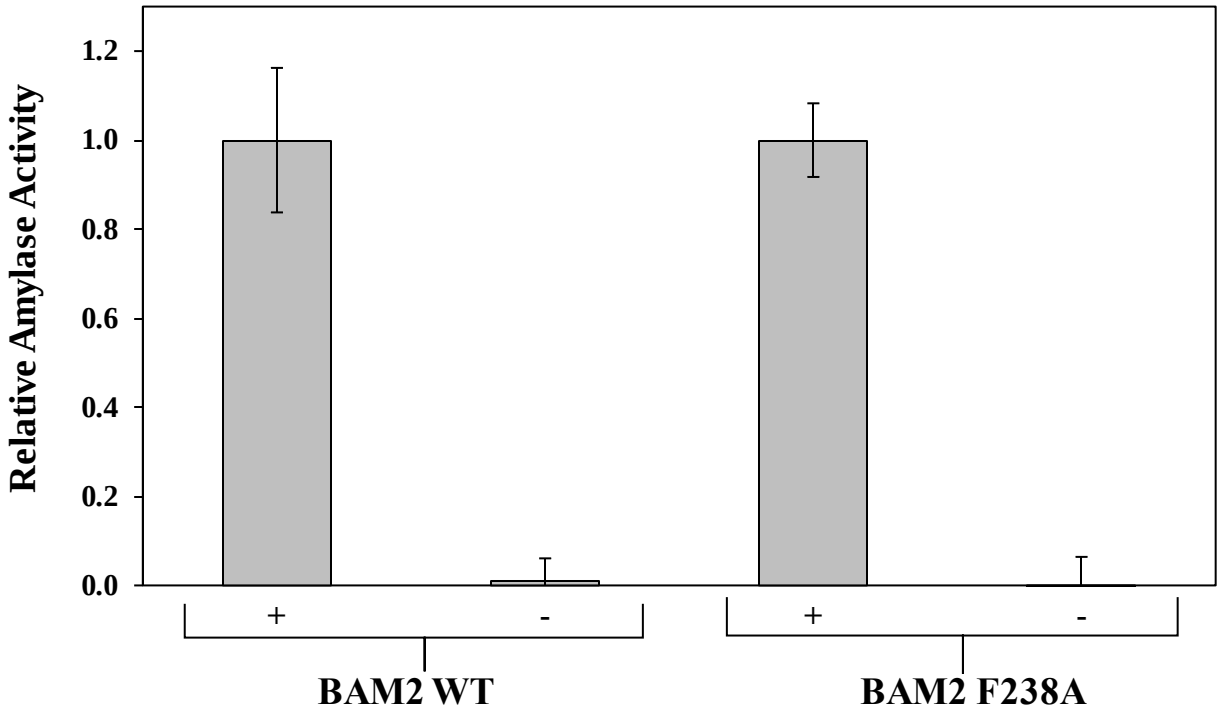

Figure 11. Enzyme Activity Assay of BAM2 WT and BAM2 F238A With (+) and Without (-) KCl. The positive controls for BAM2 WT and BAM2 F238A contained 100 mM KCl. Error bars represent one standard deviation above and below the mean (n=3). Total enzyme activity for BAM2 WT and BAM2 F238A was normalized to their respective positive controls.

Discussion

BAM2 was recently found to be one of the catalytically active BAMs (Monroe et al. 2017). Along with the discovery of its activity came several unique characteristics that distinguished BAM2 from other active paralogs. Not only is BAM2 the only BAM that requires high ionic strength in the form of KCl to become activated, it also displays sigmoidal kinetics, and cooperativity with a Hill coefficient of >3 (Monroe et al. 2017). In addition, BAM2 is the only known tetrameric BAM. BAM2 is also ancestral, as it is found in early land plants while other BAMs are not. It is important to study BAM2's structure, as BAM2 is highly conserved, and investigations of its unique structure may allude to the function of the enzyme in transitory leaf starch degradation.

A model of the tetrameric structure of BAM2 was constructed based on the crystal structure of the tetrameric sweet potato BAM5. To validate that this tetramer model is a plausible hypothesis for the actual structure of BAM2, highly conserved residues that appeared to interact in the two separate interfaces were mutagenized and their effects on the quaternary structure and activity of the protein were tested. Residue F238 did not appear to interact directly in interface B of BAM2, but was predicted to play a role in formation of the tetramer's interface B because it is perfectly and uniquely conserved in BAM2 (Figures 2 and 3). MALS analysis showed the F238A mutation resulted in a molecule with an average molecular weight of 143.8 kDa, with a ratio of calculated to expected molecular weight of 2.5:1, consistent with it being a dimer (Figure 8). This leads us to hypothesize that the true structure of BAM2 is much more compact, with subunits in closer proximity with one another in interface B than what appears in the tetramer model.

We wanted to observe the impact of mutations hypothesized to be in interface A on BAM2's quaternary structure as well. BAM2 D490R was predicted to disrupt tetramerization, as residue D490 appears to be integrated into interface A. The results of SEC MALS analysis of the BAM2 D490R mutant showed an average experimental molecular weight of 59.5 kDa, with an experimental to calculated ratio of 1:1 (Figure 8). This supports our hypothesis that this residue is in an interface, as changing the residue disrupted tetramerization. Another residue hypothesized to be in interface A was W456, and it is perfectly conserved in BAM2 (Figure 2). MALS analysis showed that the BAM2 W456A mutant had an average molecular weight of 135.8 kDa. BAM2 W456A is thus dimeric in solution, and because W456 appears in interface A, the BAM2 W456A dimer probably consists of two subunits attached by interface B. The disruption of the BAM2 tetramer in both interfaces leads us to conclude that the BAM2 tetramer model is fairly accurate, and is a reliable way of observing BAM2's structural properties even though a crystal structure is not available.

The impact of these site directed mutants on BAM2's ability to hydrolyze starch was the next focus of this study. We predicted that BAM2 would be active without a tetrameric conformation, as its homolog, sweet potato BAM5, crystallized as a tetramer but is active as a monomer (Thomas et al. 1963; Cheong et al. 1995). BAM2 W456A and BAM2 D490R both had considerably less activity than BAM2 WT (Figure 9). One notable difference between BAM2 and BAM5 is that BAM2 possesses a putative surface binding site that is necessary for catalysis (Monroe et al. 2017). Two separate glycine to methionine mutants in BAM2's surface binding site resulted in lowered activity, similar to the results of the BAM2 D490R and BAM2 W456A mutations (Monroe et al. 2017). The tetramer model oriented these two surface binding sites adjacent to one another to form a starch binding groove (Figure 1), and BAM2 D490R and

BAM2 W456A most likely disrupted the interface that holds together this groove, which destroyed BAM2's mechanism of cooperativity. We now hypothesize that this groove must remain intact for starch to bind to the adjacent starch binding surfaces of BAM2, and therefore for BAM2 to be active. There are many plausible reasons why BAM2 must maintain an intact surface binding groove, such as keeping the enzyme close to its substrate, disruption of highly stable substrates, and higher efficiency (Cuyvers et al. 2012). Further studies of BAM2 in vivo may clarify in more detail why the structure of the protein influences its function.

As previously mentioned, BAM2 F238A probably disrupted interface B of BAM2's tetrameric structure. While assays of BAM2 WT and BAM2 F238A had some variability between trials, making it difficult to draw firm conclusions regarding the kinetics of the dimer, we noticed that the BAM2 F238A mutant had a similar total activity at saturating levels of starch than wild type (Figure 9). On the other hand, the dimer that disrupted interface B (BAM2 F238A) had a higher Km than wild type, showing that it has a lower affinity for starch (Table 2). Further studies of BAM2 and BAM2 F238A kinetics may clarify more about the differences between the tetramer and the active dimer. For now, we conclude that BAM2 F238A did not disrupt interface A, allowing the enzyme to maintain its cooperativity so it could act on starch. These results show that BAM2's tetrameric structure is conserved for a particular function that is not yet clear, as disruption of the tetramer in three different mutants led to a negative impact on BAM2's activity. These conserved residues are involved in tetramerization of BAM2, and while BAM2 can be active with the starch binding groove intact, the enzyme is more active as a tetramer. This is different from our earlier hypotheses about BAM2 based on the sweet potato BAM5 characteristics, as BAM5 can be active as a monomer, but BAM2 requires a dimeric structure with an intact starch binding groove, which is another unique feature of BAM2.

We had hoped to learn more about why BAM2 needs high ionic strength through testing the active dimer's requirement for KCl. BAM2 F238A had similar total activity at saturating levels of starch compared to WT when 100 mM KCl was present, but when BAM2 F238A's activity was assayed at saturating levels of starch in the absence of KCl, it was inactive (Figure 11). We conclude that the disruption of the tetramer has no impact on BAM2's requirement for high ionic strength.

In conclusion, the tetramer model appears to be a good representation of the quaternary structure of BAM2, which can be useful for generating hypotheses about how BAM2 functions. We have reason to believe the tetramer is more condensed in reality, allowing the residues of interest in this study to truly interact with other conserved side chains on the nearest subunit. Unlike other active BAMs, BAM2 relies strongly on its quaternary structure for its catalytic activity, distinguishing it further from other active β-amylases.

.

Bibliography

Adachi M, Mikami B, Katsube T, Utsumi S (1998) Crystal structure of recombinant soybean beta-amylase complexed with beta-cyclodextrin. J Biol Chem 273: 19859–19865

Baslam M, Baroja-Fernandez E, Ricarte-Bermejo A, Sanchez-Lopez AM, Aranjuelo I, Bahaji A, Munoz FJ, Almagro G, Pujol P, Galarza R, Teixidor P, Pozueta-Romero J (2017) Genetic and isotope ratio mass spectrometric evidence for the occurrence of starch degradation and cycling in illuminated Arabidopsis leaves. PLoS ONE 12: e0171245

Berg JM, Tymoczko JL, Stryer L (2002) Biochemistry. 5th ed. WH Freeman, NY

Caffrey DR, Somaroo S, Hughes JD, Mintseris J, Huang ES (2004) Are protein–protein interfaces more conserved in sequence than the rest of the protein surface? Protein Sci 13: 190–202

Caspar T, Lin TP, Kakefuda G, Benbow L, Preiss J, Somerville C (1991) Mutants of Arabidopsis with altered regulation of starch degradation. Plant Physiol 95: 1181–1188

Cheong CG, Eom SH, Chang C, Shin DH, Song HK, Min K, Moon JH, Kim KK, Hwang KY, Suh SW (1995) Crystallization, molecular replacement solution, and refinement of tetrameric β-amylase from sweet potato. Proteins 21: 105–117

Cuyvers S, Dornez E, Delcour JA and Courtin CM (2012) Occurrence and functional significance of secondary carbohydrate binding sites in glycoside hydrolases. Critical Rev in Biotech 32: 93–107

Edner C, Li J, Albrecht T, Mahlow S, Hejazi M, Hussain H, Kaplan F, Guy C, Smith SM, Steup M, Ritte G (2007) Glucan, water dikinase activity stimulates breakdown of starch granules by plastidial β-amylases. Plant Physiol 145: 17-28

Finazzi G, Petroutsos D, Tomizioli M, Flori S, Sautron E, Villanova V, Rolland N, Seigneurin-Berny D (2015) Ions channels/transporters and chloroplast regulation. Cell Calcium 58: 86–97

Fulton DC, Stettier M, Mettler T, Vaughan CK, Li J, Francisco P, Gil M, Reinhold H, Eicke S, Messerli G (2008) β-AMYLASE4, a non-catalytic protein required for starch breakdown, acts upstream of three active β-amylases in Arabidopsis chloroplasts. Plant Cell 20: 1048-1058

Gasteiger E, Hoogland C, Gattiker A, Duvaud SE, Wilkins MR, Appel RD, Bairoch A (2005) Protein identification and analysis tools on the ExPASy server. Humana Press pp. 571-607

Hejazi M, Fettke J, Haebel S, Edner C, Paris O, Frohberg C, Steup M, Ritte G (2008) Glucan, water dikinase phosphorylates crystalline maltodextrins and thereby initiates solubilization. Plant J 55: 323-334

Hejazi M, Fettke J, Kötting O, Zeeman SC, Steup M (2010) The laforin like dual-specificity phosphatase SEX4 from Arabidopsis hydrolyzes both C6-and C3-phosphate esters introduced by starch-related dikinases and thereby affects phase transition of alpha-glucans. Plant Physiology 152:711-722

Inoue H, Nojima H, Okayama H (1990) High efficiency transformation of *Escherichia coli* with plasmids. Gene 96:23-28

Kaplan F, Guy CL (2005) RNA interference of Arabidopsis βamylase8 prevents maltose accumulation upon cold shock and increases sensitivity of PSII photochemical efficiency to freezing stress. Plant J 44: 730–743

Kaplan K, Sung DY, Guy CL (2006) Roles of β-amylase and starch breakdown during temperatures stress. Physiol Plant **126**: 120-128

Kötting O, Santelia D, Edner C, Eicke S, Marthaler T, Gentry MS, Comparot-Moss S, Chen J, Smith AM, Steup M (2009) STARCH-EXCESS4 is a laforin-like phosphoglucan phosphatase required for starch degradation in *Arabidopsis thaliana*. Plant Cell 21:334-346

Lao NT, Schoneveld O, Mould RM, Hibberd JM, Gray JC, Kavanaugh TA (1999) An Arabidopsis gene encoding a chloroplast targeted β-amylase. Plant J 20: 519–527

Li J, Francisco P, Zhou W, Edner C, Steup M, Ritte G, Bond CS, Smith SM (2009) Catalytically-inactive β-amylase BAM4 required for starch breakdown in Arabidopsis leaves is a starch-binding-protein. Arch Biochem Biophys 489: 92-98

Monroe JD, Preiss J (1990) Purification of a β-amylase that accumulates in *Arabidopsis thaliana* mutants defective in starch metabolism. Plant Physiol 94: 1033–1039

Monroe JD, Storm AR, Badley EM, Lehman MD, Platt SM, Saunders LK, Schmitz JM, Torres CE (2014) β-Amylase1 and β-Amylase3 are plastidic starch hydrolases in Arabidopsis that seem to be adapted for different thermal, pH, and stress conditions. Plant Phys 166: 1748-1763

Monroe JD, Breault JS, Pope LE, Torres CE, Gebrejesus TB, Berndsen CE, Storm AR (2017) Arabidopsis β-amylase2 is a K+-requiring, catalytic tetramer with sigmoidal kinetics. Plant Physiology, pp-01506

Nelson N (1944) A photometric adaptation of the Somogyi method for the determination of glucose. Journal of Biological Chemistry 153: 375-380

Niittylä T, Messerli G, Trevisan M, Chen J, Smith AM, Zeeman SC (2004) A previously unknown maltose transporter essential for starch degradation in leaves. Science 303: 87-89

Reinhold H, Soyk S, Šimková K, Hostettler C, Marafino J, Mainiero S, Vaughan CK, Monroe JD, Zeeman SC (2011) β-amylase-like proteins function as transcription factors in Arabidopsis, controlling shoot growth and development. Plant Cell 23: 1391-1403

Ritte G, Lloyd JR., Eckermann N, Rottmann A, Kossmann J, Steup M. (2002) The starch-related R1 protein is an α-glucan, water dikinase. Proceedings of the National Academy of Sciences 99: 7166-7171

Soyk S, Simkova K, Zürcher E, Luginbühl L, Brand LH, Vaughan CK, Wanke D, Zeeman SC (2014) The enzyme-like domain of Arabidopsis nuclear β-amylases is critical for DNA sequence recognition and transcriptional activation. Plant Cell 26:1746–1763

Streb S, Eicke S, Zeeman SC (2012) The simultaneous abolition of three starch hydrolases blocks transient starch breakdown in Arabidopsis. J Biol Chem 287: 41745-41756

Thoma JA, Koshland DE Jr, Ruscica J, Baldwin R (1963) The number of binding sites of sweet potato beta amylase. Biochem Biophys Res Commun 12: 184–188

Wang Q, Monroe J, Sjolund RD (1995) Identification and characterization of a phloem-specific β-amylase. Plant Physiology 109: 743-750

Zeeman SC, Kossmann J, Smith AM (2010) Starch: its metabolism, evolution, and biotechnological modification in plants. Annu Rev Plant Biol 61: 209-234